




Microstructural refinement of 355 aluminium alloys by ultrasonic melt treatment (UST)

Leandro Cássio de Paula¹ · Eugenio Jose Zoqui¹ 

© Springer Nature Switzerland AG 2019

Abstract

Chemical grain refining of high-silicon-content aluminium alloys, such as 355 alloy, is impaired by the high silicon content. One solution is the use of ultrasonic melt treatment (UST). This study sought to determine the duration of UST and type of horn (steel or Ti) required to achieve optimal grain refining in these alloys. Samples produced by conventional casting underwent UST for different times with steel and Ti horns and were compared with as-cast samples. For all the conditions studied, analysis of the samples showed that UST is an effective grain refining technique and yields satisfactory values of average grain size and primary and secondary dendrite arm spacing (λ_1, λ_2) as well as low porosity. The chemical composition of the samples was analysed by SEM–EDS mapping and point analysis to identify the intermetallic phases before and after UST. Best results were achieved after only 20 s of UST with a steel horn. UST for this length of time with a steel horn produced a homogeneous microstructure and possible homogeneous mechanical properties. Grain size was 160 μm ; primary dendrite arm spacing, or dendrite cell size, was 130 μm ; secondary arm spacing was approximately 18 μm ; and Vickers hardness was approximately 95 HV.

Keywords 355 aluminium alloy · Grain refining · Microstructural characterization · Ultrasonic melt treatment · Vickers hardness · Porosity

1 Introduction

The 355 aluminium alloys and their derivatives, 355.1, 355.2 and A355.2 [1], are well known and widely used to manufacture parts such as air compressor pistons, printing press bedplates, water jackets, crankcases, impellers, aircraft fittings, timing gears and jet engine compressor cases [2]. Although these alloys can be used in a wide range of applications, their mechanical properties and, therefore, use are limited by their generally large grain size. Furthermore, chemical grain refining is impaired by the poisoning effect of silicon [3]. In an attempt to achieve a small grain size and interdendritic arm spacing, several authors have developed different refining techniques for high-silicon-content aluminium alloys, such as ultrasonic melt treatment (UST) [4, 5].

Grain refining by ultrasonic treatment of the molten metal (UST) has been in use since the 1970s and allows parts to be produced at lower cost and with less complex production processes than other techniques. It can also degas molten metal, can be easily adapted to existing commercial technologies without major changes in the basic technological parameters and requires considerably shorter treatment time [6, 7]. The operating principle consists essentially of the application of acoustic waves in the 17–20 kHz frequency range to the molten metal in order to cause cavitations and mix the melt [8].

Refinement of aluminium alloys by UST holds promise for the aerospace industry. As cavitation is the main mechanism involved, the microstructure produced using this technique is free from contamination and the chemical

✉ Eugenio Jose Zoqui, zoqui@fem.unicamp.br; Leandro Cássio de Paula, leandrocp@fem.unicamp.br | ¹Materials and Manufacturing Department, School of Mechanical Engineering, University of Campinas – UNICAMP, Campinas, SP 13083-860, Brazil.



composition of the alloy remains unchanged, unlike in chemical refining [9].

The aim of the present study was to optimize the use of UST in the production of high-silicon-content aluminium alloys. The influence of UST on average grain size (GS), primary dendrite arm spacing (λ_1), secondary dendrite arm spacing (λ_2) and porosity of a 355 aluminium alloy when applied using two different horns is investigated. The results may help to determine the process parameters for large-scale application of this technique in industry.

2 Experimental procedure

Table 1 shows the chemical composition of 355.1 alloy according to the ASTM B179-17 standard specification [1] and the composition of the 355 aluminium alloy used in this study as measured with an Anacon BILL-OES spectrometer.

Ingots were produced by melting 550 g of the 355 alloy in a SiC crucible (130 mm high \times 108 mm outer diameter at the base \times 75 mm internal diameter) inside a resistive furnace. The pouring temperature was kept at 670 °C, about 50 °C above the liquidus temperature predicted by Thermo-Calc[®] simulation software. The material treated with ultrasound was heated beyond this pouring temperature to achieve the same final casting temperature for all the treatment conditions. In this way, the results would not be affected by the casting conditions, and the alloys that had been treated with ultrasound could be compared with those that had not. The ultrasonic melt treatment was performed with the liquid aluminium out of the furnace, and for this reason it required a different procedure in the heating. The longer treatment time (120 s) required the liquid aluminium to be heated to a higher temperature than the other conditions, since the same pouring temperature was required at the end of the refining treatment times. The ingots, which measured 30 mm D \times 260 mm H, were cast in a water-cooled copper mould. Thus, the longer the ultrasound treatment time, the higher the heating temperature of the aluminium, so that at the end of the ultrasound treatment the material is always poured at the same temperature.

UST was applied with a steel (AISI/SAE 4340) or titanium (Ti₆₄) horn and a Sonitron 20 kHz 2.8 kW power

supply. To identify the optimal treatment time, the alloy was poured into the water-cooled mould after treatment with ultrasound for 0, 10, 20, 30, 60, 90 and 120 s. For each of these times, UST was applied with a steel horn and a Ti horn to determine which yielded the best results. The horns were kept in contact with the liquid aluminium as shown in Fig. 1, and the temperature during the UST was measured with a K-type thermocouple.

The microstructure of samples from each ingot was characterized by conventional B&W and polarized light colour microscopy with a Leica DM ILM optical microscope. Samples were cut in the longitudinal direction approximately 75 mm from the base, embedded in Bakelite and ground with increasingly fine abrasive paper to a grit size of 4000. They were then manually polished with 1.0 and 0.35 μm solutions of alumina and further polished in a Buehler VibroMet 2 vibratory polisher with a 0.04 μm colloidal silica solution.

For the conventional B&W metallography, the samples did not need to be etched as the microstructures could be clearly seen. For the colour metallography, the samples were etched with 2% HBF₄ (Barker's solution) (30 V, 0.3 A, 180 s) under moderate, constant agitation [10]. These parameters were arrived at after several tests to determine the best values for the 355 alloy used here. B&W and colour images were obtained with a Leica optical microscope; LAS V4.3 software and an MC120 HD camera were used with ImageJ 1.46r to measure porosity. Colour images were mainly used to characterize grains. Grains with the same crystal orientation appear as areas with similar colours and shades, making it easier to identify and characterize them. This way those images were used to measure average grain size (using Hein's intercept method, ASTM E112-13 [11]), as well as the primary dendrite arm spacing— λ_1 (equivalent to dendrite cell size), that was estimated by the triangle method as shown in the example in Fig. 2a. The distances between three neighbouring dendrites were measured along a cross section perpendicular to the heat flow or in the direction of growth of the primary dendrite arm and averaged to give the primary arm spacing. Secondary dendrite arm spacing (λ_2) was obtained by averaging the distances between the side branches or arms in the direction of primary dendrite growth, as shown in Fig. 2b [12, 13].

Table 1 Chemical composition of 355.1 alloy according to the ASTM B179-17 standard specification [1] and composition of the 355 aluminium alloy used in this study (in wt%)

	Si	Cu	Mg	Fe	Mn	Zn	Ti	Al
355.1 [1]	4.5–5.5	1.0–1.5	0.45–0.6	<0.5	<0.5	<0.35	<0.25	Bal.
355	4.61	1.03	0.34	0.58	0.26	0.26	0.02	Bal.

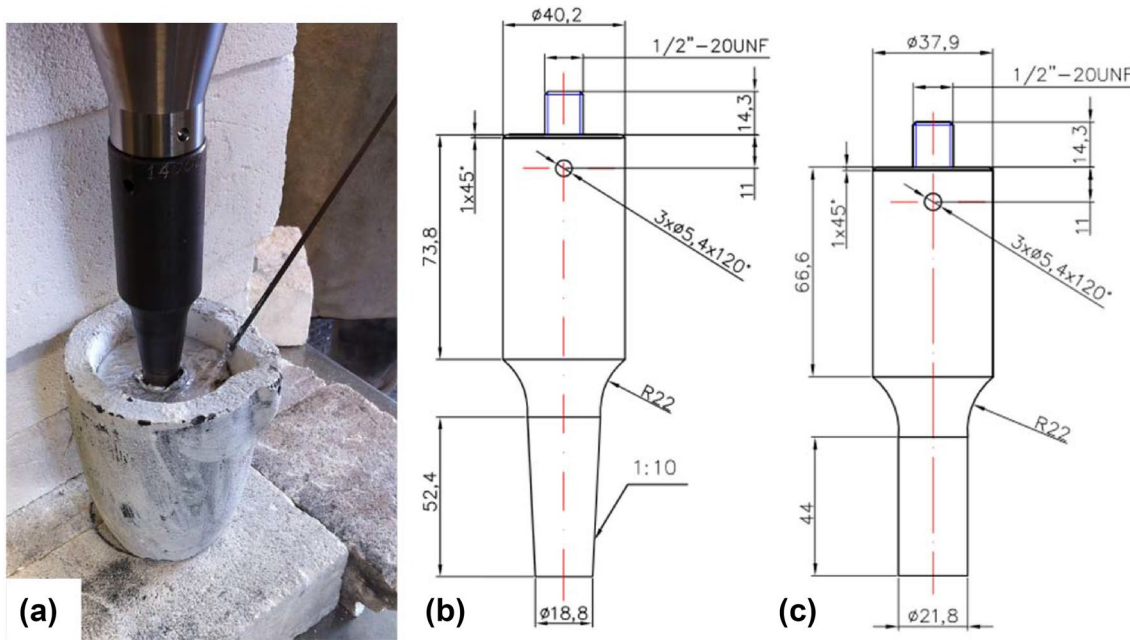


Fig. 1 **a** Setup used for the UST; schematic of **b** the steel horn and **c** the Ti horn

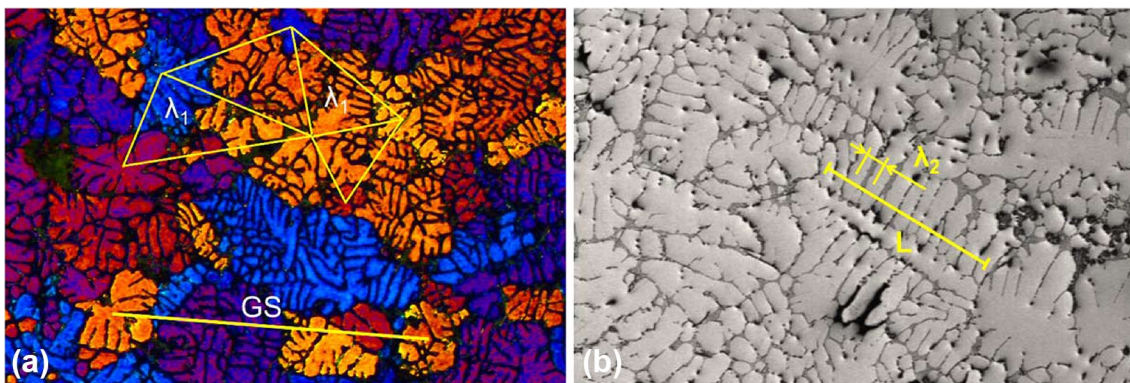


Fig. 2 Examples of the measurement procedure for the values of: **a** primary dendrite arm spacing (λ_1 —triangle method) and grain size (GS—intercept method), respectively, and **b** secondary dendrite arm spacing (λ_2) by the intercept method ($\lambda_2 = L/(n - 1)$) [12, 13]

The mechanical properties of the specimens for all the UST times and both types of horn were determined by Vickers hardness testing in a Future-Tech FV-800 under a 1 kgf load applied for 10 s. The hardness tests were performed in accordance with ASTM E384-17 [14] using cylindrical samples with a diameter of 30 mm. Tests were conducted in three regions of the specimens (the outer edge and an intermediate and a central region) so that each region could be studied in detail and an overall assessment made.

Chemical composition analysis distribution was performed by energy-dispersive X-ray spectrometry (EDS) and scanning electron microscopy (SEM) to identify the elements present in the 355 alloy. Chemical distribution

mapping and point analysis of the matrix and constituents were performed for three conditions: no UST; 30 s of UST with a steel horn; and 30 s of UST with a Ti horn.

3 Results and discussion

3.1 Microstructural characterization

Samples were characterized microstructurally to assess the influence of UST on the average grain size, λ_1 , λ_2 and porosity and the mechanical properties in terms of hardness of the 355 aluminium alloy. This information was used to assess the effectiveness of UST applied prior to casting

for each of the six durations (10, 20, 30, 60, 90 and 120 s) with Ti and steel horns using the untreated ingots as a reference.

Figure 3 shows the microstructure of the 355 alloy without UST. The colour micrograph in Fig. 3a was taken under polarized light and shows the grain size and morphology of the as-cast structure. The microstructure is coarse and dendritic with large grains formed by the expected α phase, which is surrounded and permeated by the eutectic phase, forming small (secondary dendrite) arms inside the grain. In the conventional B&W micrograph in Fig. 3b, the areas within the dotted red lines show the dendrites as a whole. The eutectic phase can be clearly seen at the dendrite boundary, where it determines the dendrite cell size (λ_1), and around the small secondary arms in the grain, where it determines the secondary dendrite spacing (λ_2). The arrows identified by the letter P show small pores, possibly contracting pores, between the dendritic arms. In the colour micrograph, all the α phase is the same colour and shade, giving an indication of the total extent of the grain. This coarse, untreated microstructure was used as a reference to assess the microstructure in the samples refined with UST.

Figure 4 shows colour micrographs of the 355 alloy taken under polarized light after 10, 20, 30, 60, 90 and 120 s of UST with steel and Ti horns. There is a decrease in grain size in relation to the untreated alloy for all the conditions tested, and the micrographs suggest that the grain refining effect becomes more marked at treatment times of between 30 and 60 s for both horn materials. However, without quantitative metallography it is impossible to establish whether both horns (steel and Ti) produce significant grain refining.

The largest average grain size ($210 \pm 45 \mu\text{m}$) after UST was observed for 10 s of treatment with a Ti horn. This represents a 16% reduction in grain size compared with the

as-cast alloy. For short periods of UST (10 and 20 s), the steel horn appears to be more effective, while for periods of 30 and 60 s, slightly smaller grains were achieved with the Ti horn. The micrographs therefore suggest that the ultrasound technique is most effective for treatment times of 20–60 s, which produce smaller grains than the other times.

For treatment times of 30 and 60 s, the reduction in average grain size is about 35% with the steel horn and 40% with the Ti horn. The grain refining effect of UST appears to vary little with treatment time when a steel horn is used, allowing better control of the process, while with the Ti horn it varies greatly. The results of detailed quantitative metallography are discussed later.

The main mechanism involved in grain refinement in UST is cavitation [9], which results in the nucleation, growth and fragmentation of dendrites during the solidification process. In fact, UST produces many high-pressure and low-pressure sites inside the molten metal: small nuclei form in the high-pressure sites and can survive if the temperature is low enough, while gas bubbles form in the low-pressure sites and emerge at the surface of the molten metal, leading to degassing. Another possible mechanism that leads to grain refinement in UST involves the formation of grains at the surface of the horn when this is immersed in the molten metal. Although the horn contact area (277 mm^2 for the steel horn and 373 mm^2 for the Ti horn) is small compared with the surface area of the molten metal (approx. 6360 mm^2), the contact between horn and molten metal is probably sufficient to produce small nuclei that detach from the horn and, if the temperature is low enough, survive in the molten metal, generating new grains during solidification. In addition to this, there is the effect of the thermal conductivity of the sonotrode that for the steel AISI/SAE 4340 is 54 W/m K and for the Ti is 19 W/m K

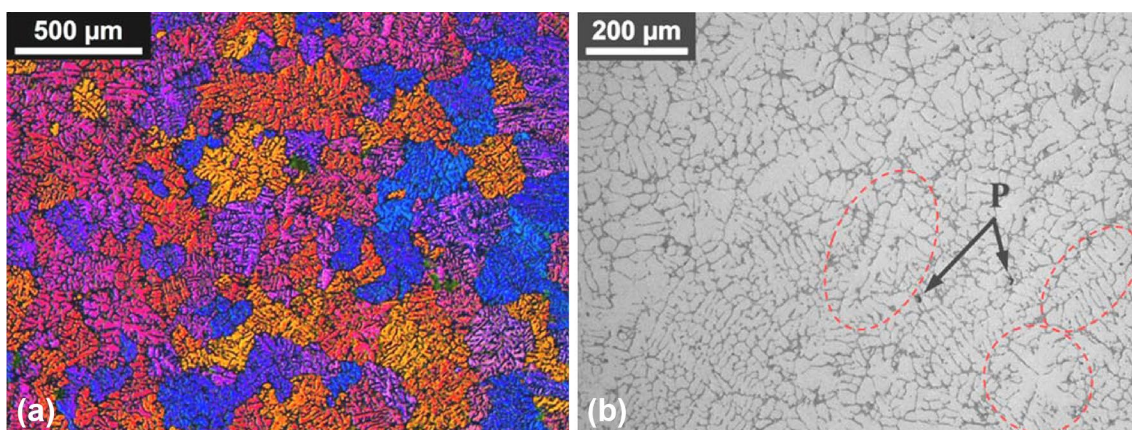


Fig. 3 Microstructure of the 355 alloy produced by conventional casting: **a** polarized light colour micrograph highlighting grain boundaries and **b** conventional B&W micrograph showing pores (P) and dendritic regions (within dotted red lines)

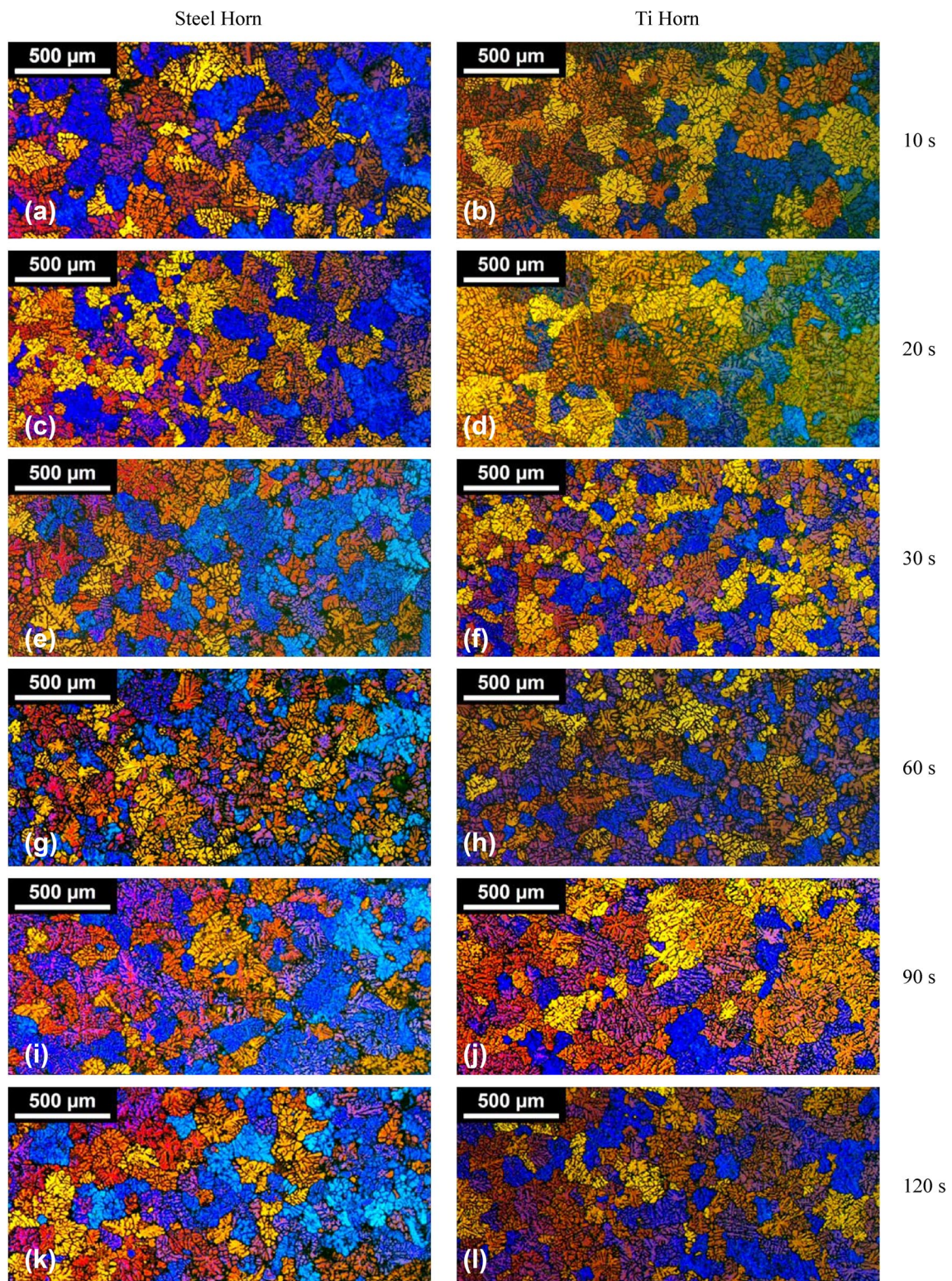


Fig. 4 Polarized light colour micrographs showing the microstructure of the 355 alloy after UST with steel and Ti horns for **a, b** 10 s; **c, d** 20 s; **e, f** 30 s; **g, h** 60 s; **i, j** 90 s; and **k, l** 120 s

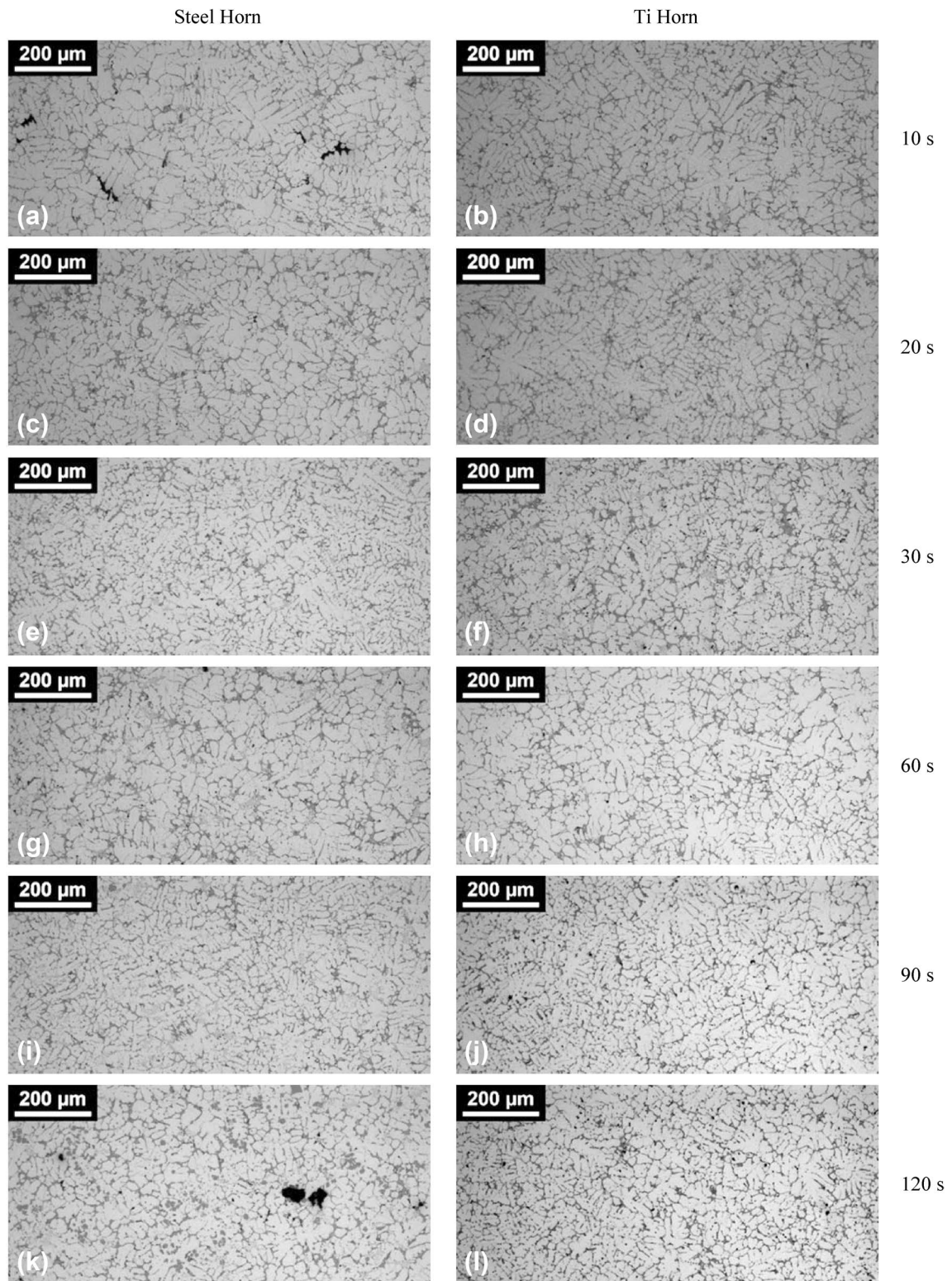


Fig. 5 Conventional B&W micrographs showing the microstructure of the 355 alloy after UST with steel and Ti horns for **a, b** 10 s; **c, d** 20 s; **e, f** 30 s; **g, h** 60 s; **i, j** 90 s; and **k, l** 120 s

Table 2 Grain size (GS), primary arm spacing (λ_1), secondary arm spacing (λ_2) and porosity (P) of the 355 alloy for all the conditions tested

UST time (s)	GS (μm)		λ_1 (μm)		λ_2 (μm)		P (%)	
	Steel horn	Ti horn	Steel horn	Ti horn	Steel horn	Ti horn	Steel horn	Ti horn
10	182 ± 39	210 ± 45	149 ± 35	182 ± 47	17 ± 4	18 ± 4	1.53 ± 0.93	0.18 ± 0.17
20	163 ± 34	178 ± 32	135 ± 38	173 ± 40	17 ± 4	19 ± 4	0.38 ± 0.27	0.19 ± 0.19
30	159 ± 28	144 ± 26	132 ± 29	153 ± 26	19 ± 5	17 ± 4	0.38 ± 0.22	0.48 ± 0.47
60	163 ± 33	149 ± 27	133 ± 32	162 ± 45	19 ± 5	18 ± 4	0.55 ± 0.23	0.06 ± 0.03
90	173 ± 33	177 ± 33	135 ± 32	170 ± 29	17 ± 4	18 ± 4	0.11 ± 0.10	0.23 ± 0.09
120	176 ± 34	169 ± 36	134 ± 26	155 ± 28	20 ± 5	16 ± 4	0.68 ± 0.59	0.21 ± 0.18
As cast	250 ± 50		192 ± 49		18 ± 4		0.4 ± 0.25	

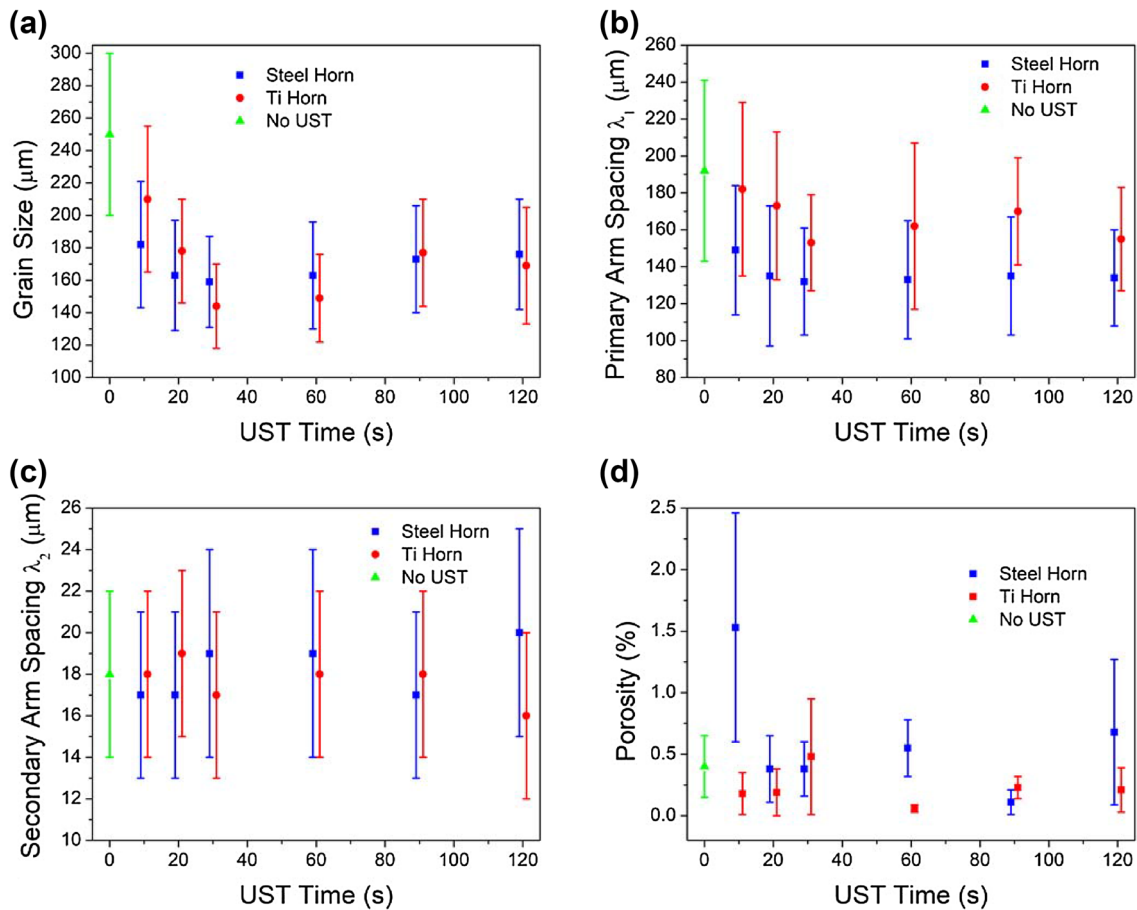


Fig. 6 Results of quantitative metallography of the 355 alloy for all the conditions tested: **a** grain size (GS); **b** primary dendrite arm spacing (λ_1); **c** secondary dendrite arm spacing (λ_2); **d** porosity (P)

at approximately 500 °C. Since the contact area of the Ti is higher compared to the steel sonotrode, the higher thermal conductivity of the steel could compensate the lower area. Thus, during UST, both cavitation and nucleation occur at the surface of the horn, and the resulting

nuclei are mixed throughout the molten metal, where they multiply and become small solidification sites [4, 9, 15].

Using the conventional B&W micrographs in Fig. 5, a similar analysis can be conducted. Comparison of Figs. 4

Table 3 Vickers hardness of the 355 alloy for all the conditions tested

UST time (s)	Vickers hardness (HV)	
	Steel horn	Ti horn
10	88.9 ± 4.7	90.8 ± 4.5
20	94.4 ± 5.2	85.9 ± 4.3
30	95.1 ± 4.9	88.7 ± 3.9
60	86.7 ± 3.6	92.8 ± 5.3
90	96.1 ± 5.1	92.1 ± 4.1
120	100.1 ± 5.7	95.9 ± 5.5
As-Cast	93.9 ± 4.0	

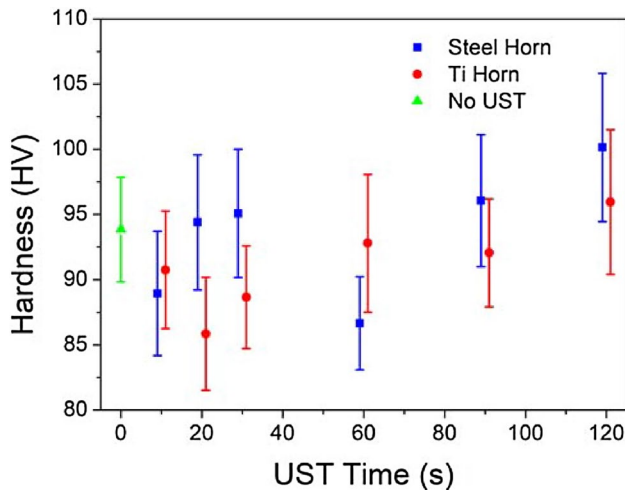


Fig. 7 Vickers hardness of the 355 alloy after ultrasonic melt treatment for all the conditions tested. The Vickers hardness for the untreated alloy is also shown

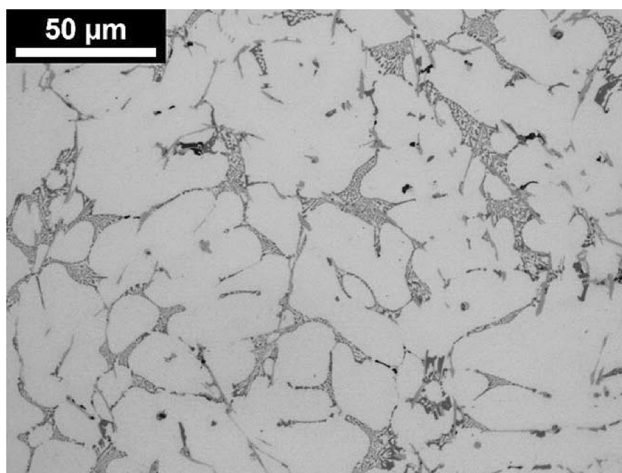


Fig. 8 Conventional B&W micrographs showing details of the microstructure of the 355 alloy produced by conventional casting

and 5 reveals that the dendrite cell size, or λ_1 , is smaller than in the as-cast structure, while λ_2 is almost the same.

The results of quantitative metallography for all the conditions tested are shown in Table 2. Porosity is included in the table as it can adversely affect the final mechanical properties. The steel horn produces a smaller grain size than the Ti horn for treatment times of 10 and 20 s. While the Ti horn produces a smaller grain size and larger λ_1 for a treatment time of 30 s (144 vs. 159 μm), as shown in Fig. 6a, b; this difference is less than the standard deviation of each measurement. As a steel horn is significantly less expensive than a Ti horn and as shorter treatment times are preferable to longer ones, a steel horn can be considered more suitable for industrial use. The results in Table 2 are shown graphically in Fig. 6, where the superiority of UST with a steel horn for shorter treatment times is evident.

The values of λ_2 shown in Table 2 (and graphically in Fig. 6c) were similar for all the conditions tested. In fact, λ_2 depends on the cooling rate during solidification after pouring and is independent of the number of nuclei generated during UST.

One of the advantages of UST is the degassing effect it has in molten metals [4–7]. However, while the porosity after UST for 10 s with a steel horn was 1.53%, the porosity after treatment for 20 s with the same horn was only 0.38%, indicating that UST did not lead to degassing, probably because the raw material used already had a low hydrogen content and little contamination, as shown in Fig. 6d.

To evaluate the likely mechanical properties of parts produced by conventional casting and refined with UST, the Vickers hardness (HV) was measured for all the conditions tested. Vickers hardness testing is commonly used to evaluate materials and control manufacturing processes. Although a simple test, it is important because hardness can be correlated with tensile strength, machinability, wear resistance, toughness and ductility [14]. Table 3 summarizes the results of the hardness tests, which are also shown graphically in Fig. 7. Overall, the hardness of the samples varied little with treatment time and horn material, although slightly higher values were achieved with the steel horn in some cases.

Samples treated with ultrasound for 30 s using a steel horn had higher hardness values than any of the samples treated with a Ti horn (apart from those treated for 120 s) or the samples in the as-cast condition. This can be explained by the refining of the microstructure shown in Figs. 5 and 6, where the average grain size and λ_1 are smaller after UST with the steel horn. In particular in the condition of 120 s, intermetallic phases may have contributed to high results in the hardness values, due to the coarse silicon particles observed. For a treatment time

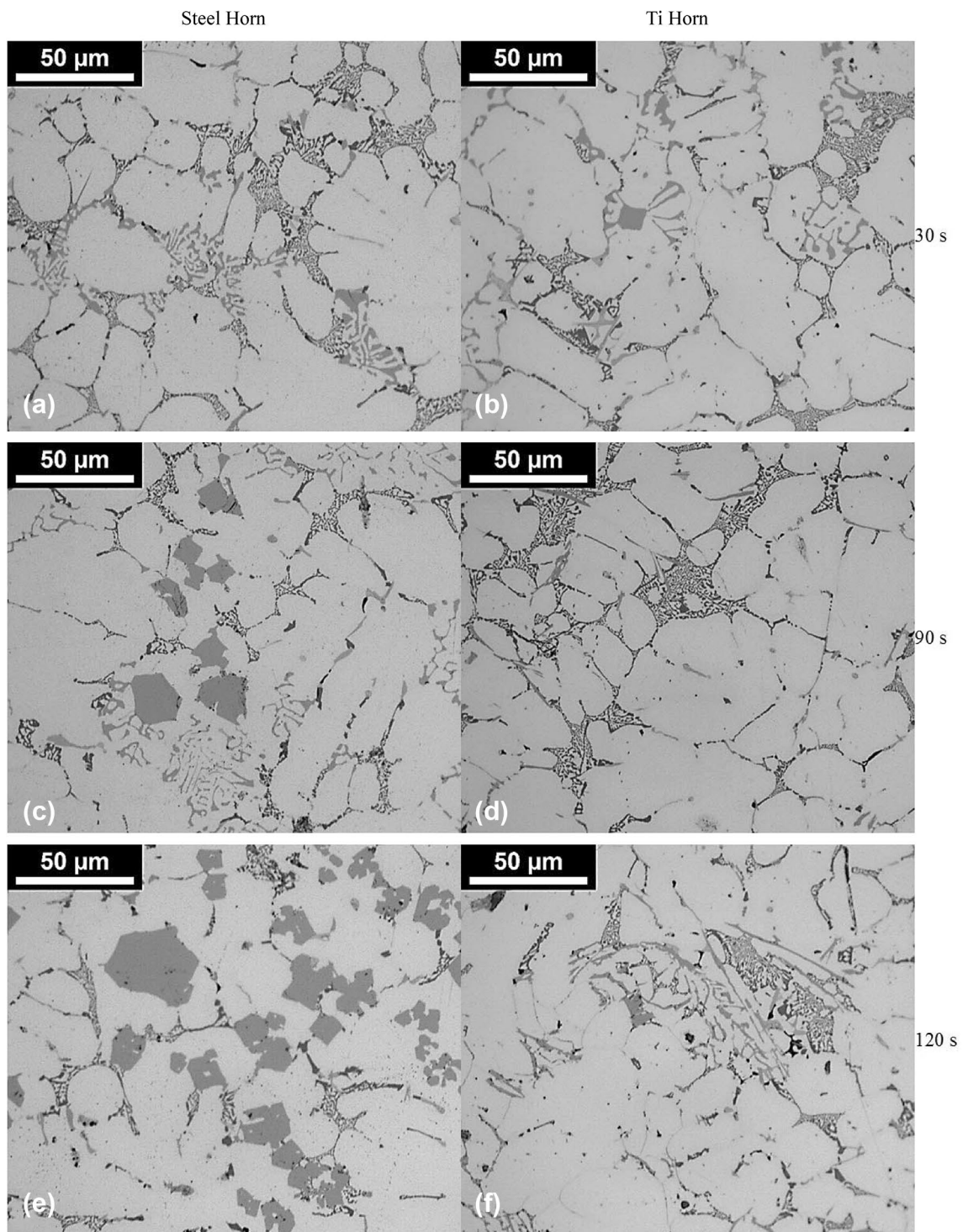


Fig. 9 Conventional B&W micrographs of atypical regions showing details of the microstructure of the 355 alloy after UST with steel and Ti horns for **a, b** 30 s; **c, d** 90 s; and **e, f** 120 s

of 10 s, the hardness was lower than in the as-cast alloy regardless of the type of horn used, highlighting the ineffectiveness of UST when applied for this short time.

In all the microstructural analyses, the standard deviation was generally similar, confirming the homogeneity of the 355 alloy processed using UST. The superior results

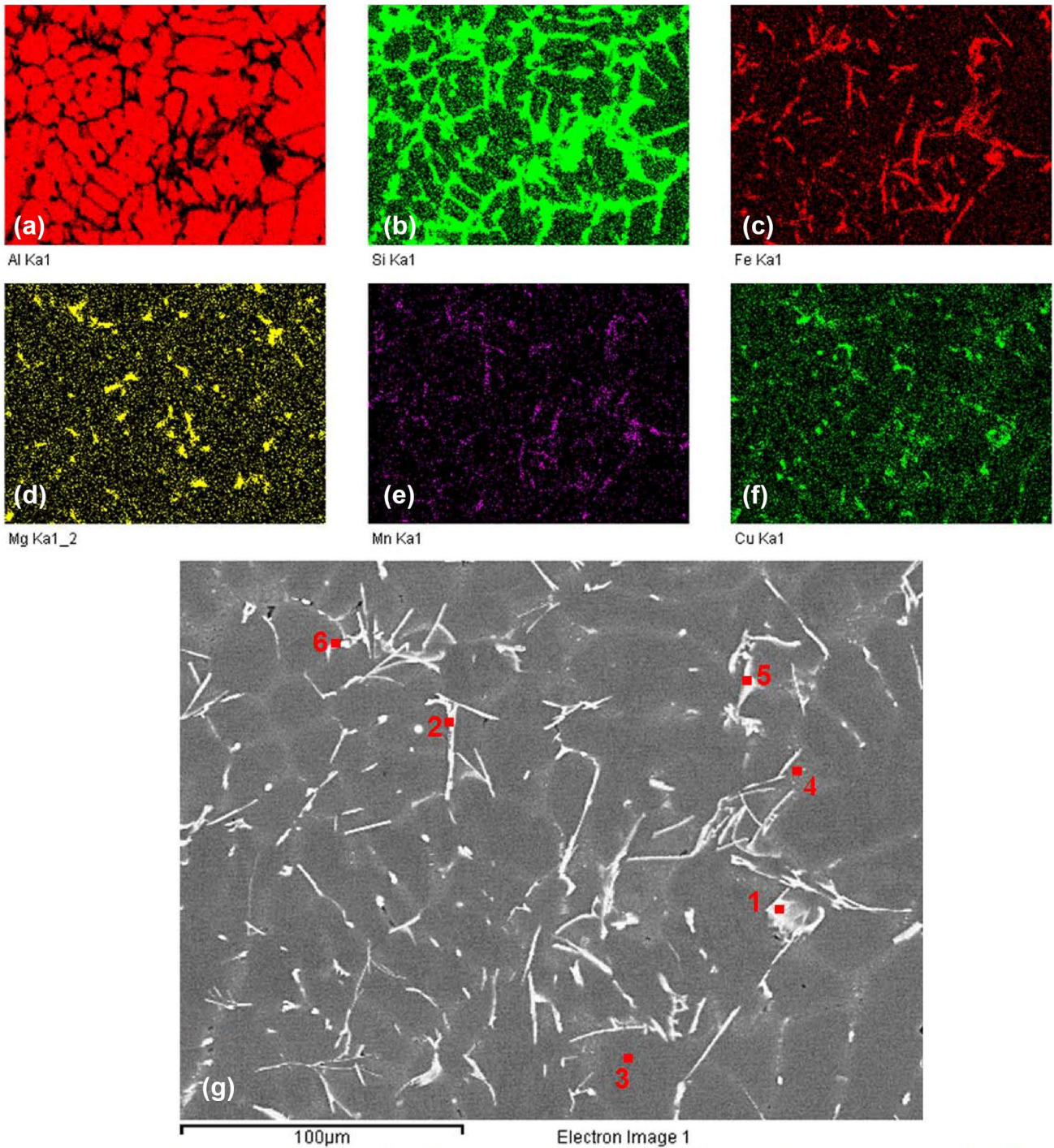


Fig. 10 EDS elemental maps of **a** Al, **b** Si, **c** Fe, **d** Mg, **e** Mn and **f** Cu in the as-cast 355 alloy and **g** SEM image

achieved with the steel horn and the low cost of this material make this the preferred horn for industrial use.

3.2 Intermetallic concentration and morphology

Identification of the intermetallic phases of the 355 alloy for the conditions studied was one of the objectives of

this work. With the aid of conventional B&W micrographs, SEM and EDS analysis allowed the microstructures for each condition to be observed.

The B&W micrographs in Figs. 8 and 9 show the typical microstructure of the 355 alloy without UST (Fig. 8) and after 30, 90 and 120 s of UST with steel and Ti horns (Fig. 9). To analyse the influence of the treatment on the chemical

Table 4 Results (in wt% and at.%) of EDS point analysis of the 355 alloy produced by conventional casting

Point		Al	Si	Fe	Mg	Mn	Cu	Calculated formula	Suggested formula
1	wt%	50.00	23.19	14.71	0.31	4.12	7.06	$Al_{25}Si_{11}Fe_4Cu_2Mn$	Al–Si(FeMnCu)
	at.%	59.00	26.29	8.39	0.41	2.39	3.54		
2	wt%	75.37	14.06	6.89	–	1.98	1.70	$Al_6Fe_{0.2}Si$	Al–Fe–Si
	at.%	80.27	14.38	3.55	–	1.04	0.77		
3	wt%	98.70	0.83	–	–	0.20	0.27	Al	Al
	at.%	98.99	0.80	–	–	0.10	0.11		
4	wt%	73.19	25.72	–	0.14	–	0.95	Al_3Si	Al–Si
	at.%	74.34	25.10	–	0.16	–	0.41		
5	wt%	57.07	20.76	12.50	0.62	3.70	5.05	$Al_{31}Si_{11}Fe_3CuMn$	Al–Si(FeMnCu)
	at.%	65.07	22.74	6.89	0.78	2.07	2.44		
6	wt%	76.92	1.81	–	0.99	–	19.16	$Al_{10}Cu$	Al–Cu
	at.%	87.52	1.98	–	1.25	–	9.26		

The points used are shown in red in Fig. 10g

composition and identify any intermetallic phases in the 355 alloy, EDS analysis was performed on the material in the as-cast condition (Fig. 10 and Table 4), after 30 s of UST with a steel horn (Fig. 11 and Table 5) and after 30 s of UST with a Ti horn (Fig. 12 and Table 6). The analysis was performed using SEM–EDS mapping and point composition analysis of the Al matrix and constituents. The points used in the analysis are shown in the SEM images in Figs. 10g, 11g and 12g.

The conventional B&W micrographs in Fig. 9 show atypical regions with clusters of silicon particles in the microstructure of the 355 alloy after UST with steel and Ti horns for (a, b) 30 s; (c, d) 90 s; and (e, f) 120 s, highlighting the importance of reducing the duration of UST as much as possible to avoid the formation of large silicon particles that can adversely affect the final mechanical properties.

Figure 10 shows the chemical composition of the α aluminium matrix, eutectic and intermetallic phases. The highest elemental concentrations were for Al, Si, Fe, Cu, Mn and Mg. A similar result was obtained in the point composition analysis. Figure 10a shows the chemical composition of the matrix, which consists primarily of Al. Figure 10b–f shows that the eutectic consists basically of a high percentage of Si, Fe (also in a high percentage) and Mg, Mn and Cu (in lower percentages). Ni, Zn and Cr are distributed in low quantities throughout the material and have no impact on the formation of intermetallic compounds.

As already mentioned, Fig. 10g shows the points used in the point composition analysis. The corresponding results are shown in Table 4 and compare favourably with the results of the chemical mapping. At point 3, the Al content in the matrix of the material is 98.7%. The other points represent the intermetallic compounds, and all have an Si content of approximately 15% and high Fe and Cu contents.

The results of the point analysis enabled the formulae of the intermetallic phases to be calculated by the stoichiometric method. The resulting formulae, which are shown in Table 4, are $Al_xSi_xFe_xCu_xMn$; $Al_6Fe_{0.2}Si$; Al_3Si ; and $Al_{10}Cu$. The $Al_xSi_xFe_xCu_xMn$ intermetallic phase was present with two different elemental ratios.

The results of the chemical analysis and the point analysis of the alloy after 30 s of UST with a steel horn are shown in Fig. 11 and Table 5, respectively. They are very similar to the results for the alloy in the as-cast condition, and the elements with the highest concentrations for both types of analysis are Al, Si, Fe, Cu, Mn and Mg.

Figure 11a shows that the matrix is composed basically of Al, as observed at point 1 in the point analysis. Si is the main constituent of the eutectic phase, which also contains Fe, Mg, Mn and Cu, as shown in Fig. 11b–f, Cu being present in higher concentrations. The intermetallic compounds have a similar composition to those found in the untreated alloy and contain Fe and Mn. The formulae calculated for the respective intermetallics are $Al_{22}Fe_3Si_3Mn$, $Al_{24}Si_3Cu_3Mg$, Al_xFe_xSi and Al_xSi .

The results of the analysis of the alloy after 30 s of UST with a Ti horn are shown in Fig. 12 and Table 6 and are similar to those for the alloy treated for the same time with a steel horn. The matrix, eutectic and intermetallic constituents have similar chemical compositions as well as Chinese scripts. The formulae calculated for this condition, which are shown in Table 6, are $Al_xFe_xSi_xMn$, $Al_{36}Cu_7SiMg$, $Al_{36}Fe_6Si_5CuMn$, Al_xFe_xSi and Al_xSi .

Some intermetallics and phases deserve a more detailed explanation. For example, the intermetallics with the formula $Al_xFe_xSi_xMn$ observed after 30 s of UST with steel and Ti horns (points 2 in Fig. 11g and 1, 3, 9 and 10 in Fig. 12g, respectively) were identified in the literature as $Al_{24}Si_2(FeMn)_6$ and $Al_{15}Si_2(FeMn)_3$ [16–18]. This Fe-rich intermetallic can have a polyhedral or

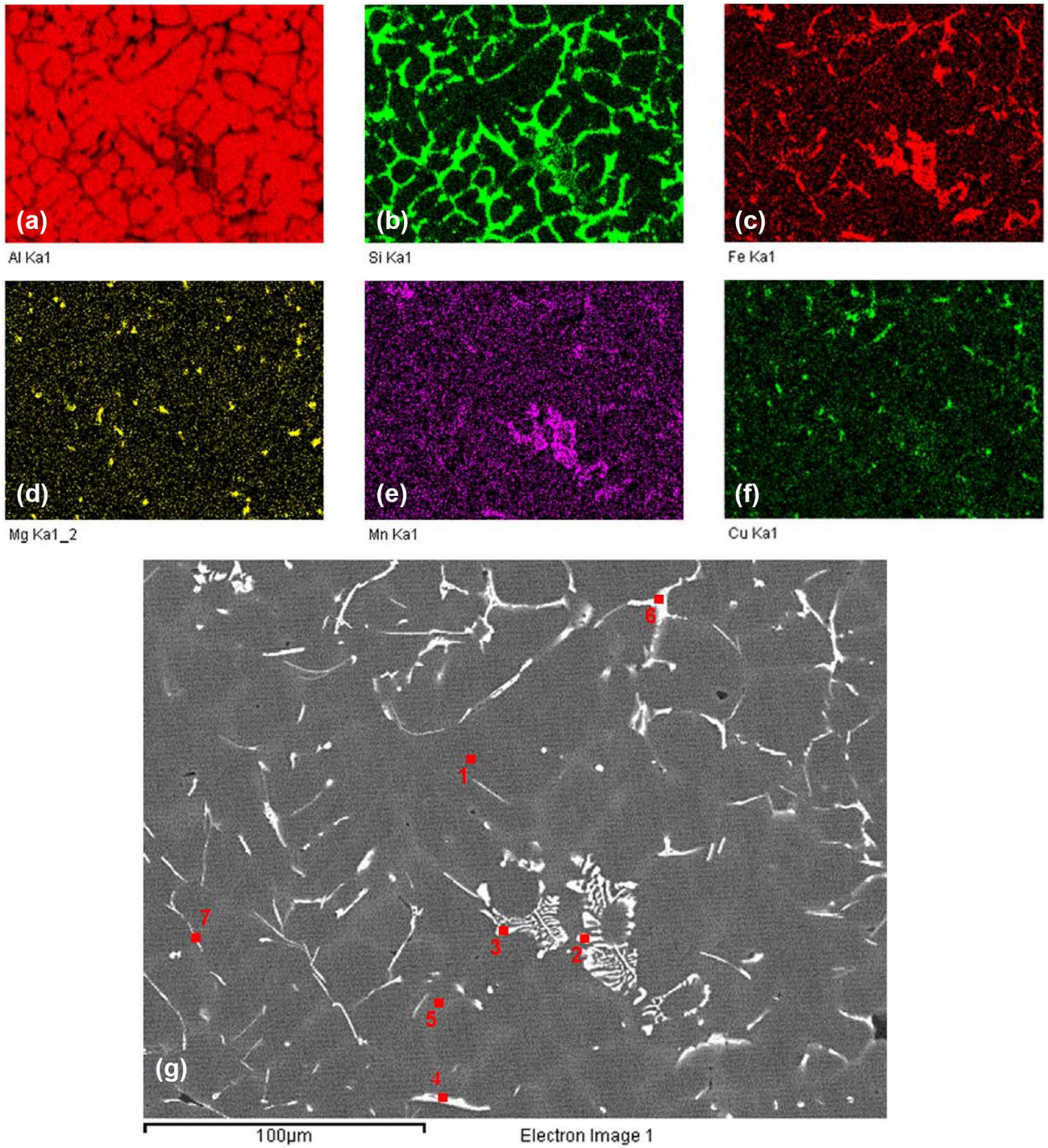


Fig. 11 EDS elemental maps of **a** Al, **b** Si, **c** Fe, **d** Mg, **e** Mn and **f** Cu in the 355 alloy after 30 s ultrasonic melt treatment with a steel horn and **g** SEM image

Table 5 Results (in wt% and at.%) of EDS point analysis of the 355 alloy after 30 s ultrasonic melt treatment with a steel horn

Point		Al	Si	Fe	Mg	Mn	Cu	Calculated formula	Suggested formula
1	wt%	98.39	0.82	–	–	–	0.45	Al	Al
	at.%	99.01	0.79	–	–	–	0.19		
2	wt%	63.42	8.79	19.51	–	5.97	1.40	Al ₂₂ Fe ₃ Si ₃ Mn	Al–Si(FeMn)
	at.%	74.77	9.96	11.11	–	3.46	0.70		
3	wt%	76.56	8.08	9.90	–	3.51	1.28	Al ₁₀ Fe _{0.6} Si	Al–Fe–Si
	at.%	83.79	8.50	5.23	–	1.89	0.59		
4	wt%	55.31	23.62	17.18	–	3.50	0.39	Al _{2.5} Fe _{0.4} Si	Al–Fe–Si
	at.%	62.72	25.73	9.41	–	1.95	0.19		
5	wt%	68.51	28.06	0.99	1.03	0.24	1.17	Al ₃ Si	Al–Si
	at.%	70.12	27.59	0.49	1.17	0.12	0.51		
6	wt%	66.39	7.61	3.45	2.50	0.62	18.91	Al ₂₄ Si ₃ Cu ₃ Mg	Al–Cu–Mg–Si
	at.%	76.77	8.45	1.93	3.21	0.35	9.28		
7	wt%	84.82	10.38	2.54	–	0.57	1.20	Al ₉ Si	Al–Si
	at.%	87.62	10.30	1.27	–	0.29	0.53		

The points used are shown in red in Fig. 11g

Chinese-script shape and is usually present within the Al matrix (inside the grain), its shape being defined by the solidification sequence. For example, the intermetallic will have a polyhedral shape if the Al_xFe_xSi_xMn phase forms before the Al phase starts to solidify; if the Al solidifies before the Al_xFe_xSi_xMn phase, the intermetallic will have a Chinese-script shape [16, 17]. While in previous works, it was shown that some intermetallics with a Chinese-script shape had a composition Al_xSi_xFe_xCu_xMn, in this work intermetallics with this composition had a plate-like morphology, as observed at points 1 and 5 in Fig. 10g and point 2 in Fig. 12g [19].

In the SEM images in Figs. 11g and 12g, intermetallic with a Chinese-script shape can be observed. This intermetallic can also be seen in the black-and-white micrographs in Fig. 9a, c, e and 9b, d, f, which shows the microstructure after 30, 90 and 120 s of UST with steel and Ti horns, respectively. Intermetallic with a polyhedral shape can be observed in greater quantities in Fig. 9c, e, corresponding to 90 s and 120 s of UST with a steel horn.

Literature also reports that the cavitation corrosion phenomena could occur leading to the partial melting of the sonotrode material and consequent contamination of the molten metal, forming Al_xMe_y phase. In fact the polyhedral AlSiFeMn phase observed for long UST time (Al₂₄Si₂(FeMn)₆ and Al₁₅Si₂(FeMn)₃) could be consequence of the contamination, highlighting the importance in use the UST technique for short periods of time [4, 20].

Another intermetallic that is worthy of note is Al_xFeSi_x, which is generally identified in the literature as Al₅FeSi with a thin, plate-like morphology and is found mainly at the grain boundary [16]. The intermetallic Al_xFeSi_x in the

present study had a similar shape and was present under all three conditions studied: no UST; UST with a steel horn; and UST with a Ti horn [16].

Al_xSi particles were found in regions without any intermetallics and between the grain boundaries. These regions are characterized by a whitish colour in Figs. 10g, 11g and 12g, which correspond to the three conditions analysed. Finally, the intermetallic Al_xCu was found only in the alloy produced by conventional casting and had a plate-like morphology, indicating that the cavitation in the liquid metal produced by the UST caused this intermetallic to melt completely and the resulting copper to spread extensively, preventing the formation of this compound during solidification. In contrast, the intermetallic Al_xSi_xCu_xMg was found in the alloy after 30 s or more of UST with either horn. This may corroborate the finding that the intermetallic Al_xSi_xCu_xMg is formed from Al_xCu, as the former generally grows next to clusters of Al₂Cu [19].

These findings suggest that there are no significant differences in the various intermetallics found for the different UST conditions. What does change, however, is their shape: while they have a needle-like morphology in the as-cast condition, after UST they are smaller, more dispersed, regular and blunt, characteristics that can generally improve the final mechanical properties. This, together with the smaller grain size made possible by UST, suggests that this type of melt treatment could be used to improve the mechanical properties of 355 alloy even when it has not been heat-treated. To confirm this, however, further work is required to compare the mechanical properties of the alloy for the different conditions tested here.

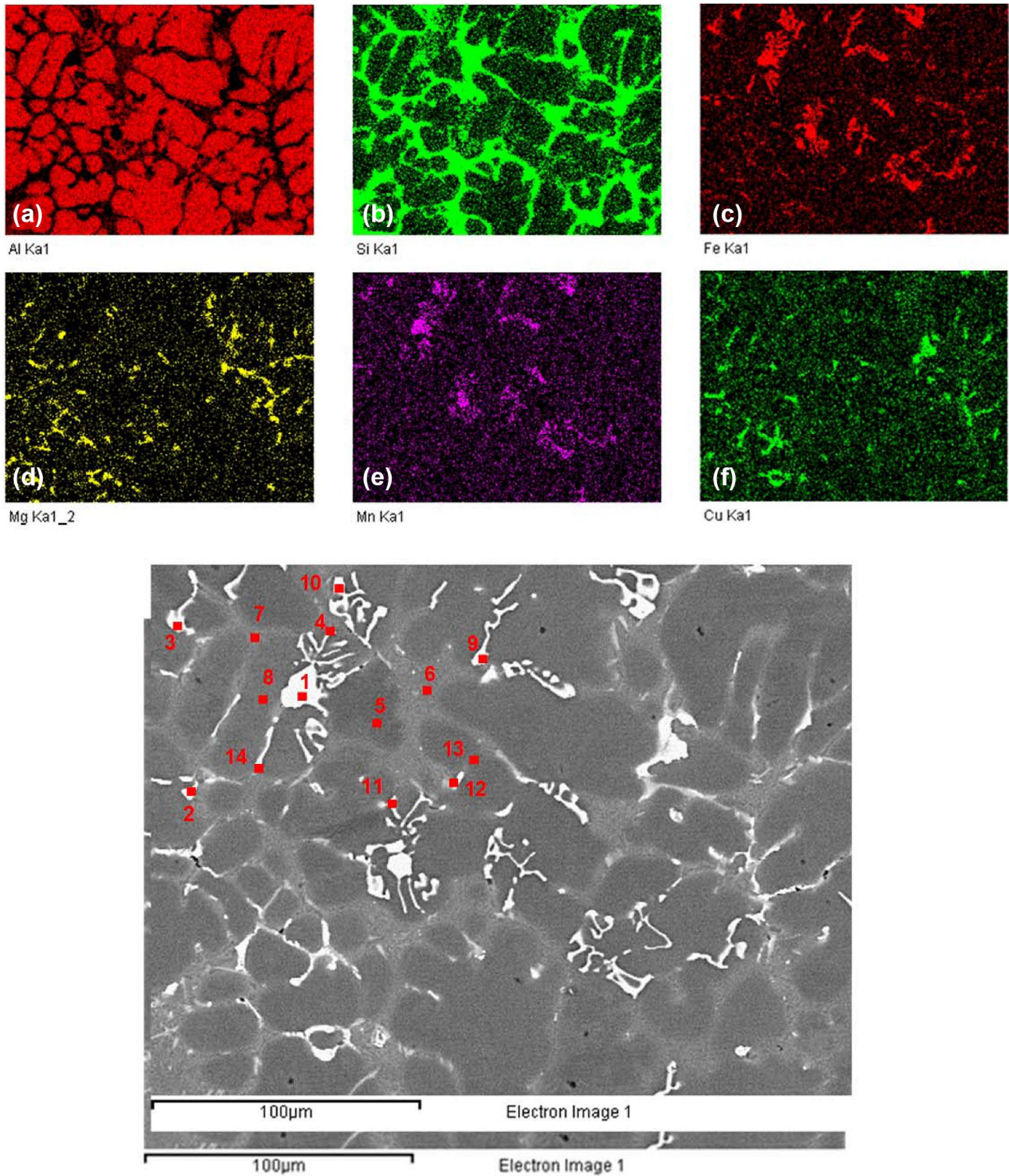


Fig. 12 EDS elemental maps of **a** Al, **b** Si, **c** Fe, **d** Mg, **e** Mn and **f** Cu in the 355 alloy after 30 s UST with a Ti horn and **g** SEM image

4 Conclusions

The purpose of this study was to identify from a wide range of UST times the treatment time that optimizes grain

refinement of 355 alloy and to determine whether a steel or Ti horn yields the best results. The findings can be used as a reference for future studies of other aluminium alloys and can thus indirectly help to reduce processing time

Table 6 Results (in wt% and at.%) of EDS point analysis of the 355 alloy after 30 s UST with a Ti horn

Point		Al	Si	Fe	Mg	Mn	Cu	Calculated formula	Reference
1	wt%	61.81	8.07	19.23	–	8.70	0.66	Al ₁₄ Fe ₂ Si ₂ Mn	Al–Si(FeMn)
	at.%	74.11	9.30	11.14	–	5.12	0.34		
2	wt%	61.43	8.93	20.13	0.92	3.45	5.14	Al ₃₆ Fe ₆ Si ₅ CuMn	Al–Si(FeMnCu)
	at.%	72.58	10.14	11.49	1.21	2.00	2.58		
3	wt%	62.55	8.72	19.34	–	6.71	1.78	Al ₁₉ Fe ₃ Si ₃ Mn	Al–Si(FeMn)
	at.%	74.18	9.93	11.08	–	3.91	0.90		
4	wt%	76.83	5.85	11.89	–	3.57	1.52	Al ₁₄ FeSi	Al–Fe–Si
	at.%	84.81	6.20	6.34	–	1.94	0.71		
5	wt%	98.29	1.12	–	–	–	0.59	Al	Al
	at.%	98.67	1.08	–	–	–	0.25		
6	wt%	77.61	20.87	–	0.18	0.20	1.15	Al ₄ Si	Al–Si
	at.%	78.84	20.37	–	0.20	0.10	0.50		
7	wt%	66.49	32.53	–	0.19	–	0.80	Al ₂ Si	Al–Si
	at.%	67.65	31.79	–	0.21	–	0.35		
8	wt%	98.48	0.79	–	–	–	0.73	Al	Al
	at.%	98.93	0.76	–	–	–	0.31		
9	wt%	65.79	8.05	17.20	–	6.26	2.01	Al ₂₁ Fe ₃ Si ₃ Mn	Al–Si(FeMn)
	at.%	76.71	9.02	9.69	–	3.58	1.00		
10	wt%	63.28	8.20	19.91	–	5.88	2.23	Al ₂₂ Fe ₃ Si ₃ Mn	Al–Si(FeMn)
	at.%	74.79	9.31	11.37	–	3.41	1.12		
11	wt%	70.26	8.06	14.49	0.85	2.96	3.38	Al ₉ FeSi	Al–Fe–Si
	at.%	79.09	8.72	7.88	1.06	1.64	1.62		
12	wt%	65.98	2.19	–	1.67	–	30.16	Al ₃₆ Cu ₇ SiMg	Al–Cu–Mg–Si
	at.%	79.74	2.54	–	2.24	–	15.48		
13	wt%	97.91	1.34	–	–	–	0.35	Al	Al
	at.%	98.55	1.30	–	–	–	0.15		
14	wt%	79.75	5.80	9.58	–	1.63	3.24	Al ₁₄ Fe _{0.8} Si	Al–Fe–Si
	at.%	86.57	6.05	5.02	–	0.87	1.49		

The points used are shown in red in Fig. 12g

and the amount of resources needed as well as potential processing errors.

The results show that UST is an alternative grain refinement technique that can be used with 355 alloy parts and that the optimal treatment time under the conditions used here was 20–30 s for both Ti and steel horns. However, as steel is much cheaper than Ti, the present authors recommend the use of a steel horn. Longer treatment times failed to produce any improvements in the microstructure, and the steel horn yielded homogeneous results even with short treatment times. When this type of horn was used, the refined 355 alloy had a grain size of 160 μm , λ_1 (or dendrite cell size) of 130 μm , λ_2 of approximately 18 μm and HV hardness of approximately 95. Homogeneity after UST was greater than in the as-cast condition, as confirmed by EDS and SEM. The intermetallics identified in the samples for the strategic conditions analysed were consistent with those reported in the literature.

Acknowledgements The authors would like to thank the Brazilian research funding agencies FAPESP (Fundação de Amparo à Pesquisa do Estado de São Paulo—Project 2015/22143-3), CNPq (Conselho Nacional de Desenvolvimento Científico e Tecnológico—PQ 304921/2017-3) and CAPES (Coordenação de Aperfeiçoamento de Pessoal de Nível Superior—Brasil (CAPES)—Finance Code 001) for providing financial support for this study. The authors are also indebted to the Faculty of Mechanical Engineering at the University of Campinas and Sonitron Ultra Sônica Ltda.

Funding FAPESP (Fundação de Amparo à Pesquisa do Estado de São Paulo—Project 2015/22143-3; CNPq (Conselho Nacional de Desenvolvimento Científico e Tecnológico—PQ 304921/2017-3 and CAPES (Coordenação de Aperfeiçoamento de Pessoal de Nível Superior—Brasil (CAPES)—Finance Code 001.

Compliance with ethical standards

Conflict of interest The authors declare that they have no conflict of interest.

Human and animals rights There is no use of humans and/or animals as subject in this research.

Informed consent The corresponding author, Prof Eugênio José Zoqui and his PhD student Leandro Cássio de Paula (first author) are the sole responsible for the information presented in this paper.

References

1. ASTM Standard B179-17 (2017) Standard specification for aluminum alloys in ingot and molten forms for castings from all casting processes. ASTM International, West Conshohocken. <https://doi.org/10.1520/b0179-17>
2. Davies JR (ed) (1993) Aluminum and aluminum alloys. ASM specialty handbook. ASM International, Russell Township, p 784. ISBN 978-0-87170-496-2
3. Lee YC, Dahle AK, StJohn DH, Hutt JEC (1999) The effect of grain refinement and Silicon content on grain formation in hypoeutectic Al–Si alloys. *Mater Sci Eng A* 259(1):43–52. [https://doi.org/10.1016/S0921-5093\(98\)00884-3](https://doi.org/10.1016/S0921-5093(98)00884-3)
4. Eskin GI (1998) Ultrasonic treatment of light alloy melts. Gordon and Breach Science Publishers, Amsterdam, pp 18–60
5. Srivastava N, Chaudhari GP, Qian M (2017) Grain refinement of binary Al–Si, Al–Cu and Al–Ni alloys by ultrasonication. *J Mater Proc Technol* 249:367–378. <https://doi.org/10.1016/j.jmatprotec.2017.06.024>
6. Fan Z (2002) Semisolid metal processing. *Int Mater Rev* 47(2):49–85. <https://doi.org/10.1179/095066001225001076>
7. Eskin GI (2001) Broad prospects for commercial application of the ultrasonic (cavitation) melt treatment of light alloys. *Ultrason Sonochem* 8(3):319–325. [https://doi.org/10.1016/s1350-4177\(00\)00074-2](https://doi.org/10.1016/s1350-4177(00)00074-2)
8. Zhang L, Eskin DG, Katgerman L (2011) Influence of ultrasonic melt treatment on the formation of primary intermetallics and related grain refinement in aluminum alloys. *J Mater Sci* 46(15):5252–5259. <https://doi.org/10.1007/s10853-011-5463-2>
9. Li J, Momono T (2005) Effect of ultrasonic output power on refining the crystal structures of ingots and its experimental simulation. *J Mater Sci Technol* 21(1):47–52
10. Voort GFV (ed) (2004) Solidification structures of aluminum alloys. In: ASM handbook, metallography and microstructure, vol 9. ASM International, Materials Park, OH, pp 107–115. <https://doi.org/10.31399/asm.hb.v09.a0003727>
11. ASTM Standard E112-13 (2013) Standard test methods for determining average grain size, ASTM International, West Conshohocken. <https://doi.org/10.1520/e0112-13>
12. Çadirli E, Gündüz M (2000) The directional solidification of Pb–Sn alloys. *J Mater Sci* 35(15):3837–3848. <https://doi.org/10.1023/A:1004829413966>
13. Gündüz M, Çadirli E (2002) Directional solidification of aluminum–copper alloys. *Mater Sci Eng A* 327(2):167–185. [https://doi.org/10.1016/S0921-5093\(01\)01649-5](https://doi.org/10.1016/S0921-5093(01)01649-5)
14. ASTM Standard E384-17 (2017) Standard test methods for microindentation hardness of materials. ASTM International, West Conshohocken. <https://doi.org/10.1520/e384-17>
15. Atamanenko TV, Eskin DG, Zhang L, Katgerman L (2010) Criteria of grain refinement induced by ultrasonic melt treatment of aluminum alloys containing Zr and Ti. *Metall Mater Trans A* 41A(8):2056–2066. <https://doi.org/10.1007/s11661-010-0232-4>
16. Irizalp SG, Saklakoglu N (2014) Effect of Fe-rich intermetallics on the microstructure and mechanical properties of thixoformed A380 aluminum alloy. *Eng Sci Technol Int J* 17(2):58–62. <https://doi.org/10.1016/j.jestch.2014.03.006>
17. Dinnis CM, Taylor JA, Dahle AK (2005) As-cast morphology of iron–intermetallics in Al–Si foundry alloys. *Scr Mater* 53(8):955–958. <https://doi.org/10.1016/j.scriptamat.2005.06.028>
18. Ji S, Yang W, Gao F, Watson D, Fan Z (2013) Effect of iron on the microstructure and mechanical property of Al–Mg–Si–Mn and Al–Mg–Si diecast alloys. *Mater Sci Eng A* 564A:130–139. <https://doi.org/10.1016/j.msea.2012.11.095>
19. Mohamed AMA, Samuel AM, Samuel FH, Doty HW (2009) Influence of additives on the microstructure and tensile properties of near-eutectic Al–10.8%Si cast alloy. *Mater Des* 30(10):3943–3957. <https://doi.org/10.1016/j.matdes.2009.05.042>
20. Eskin GI, Eskin DG (2014) Ultrasonic treatment of light alloys melts, 2nd edn. CRC Press, Boca Raton, FL, p 346. <https://doi.org/10.1201/b17270>

Publisher's Note Springer Nature remains neutral with regard to jurisdictional claims in published maps and institutional affiliations.